Receptive field properties of neurons in the macaque Anterior Intraparietal area.

Maria C Romero, Peter Janssen

Laboratorium voor Neuro- en Psychofysiologie, KU Leuven, Belgium

Running head:

Receptive fields in AIP.

Corresponding author:

Peter Janssen MD PhD

Laboratorium voor Neuro- en Psychofysiologie, Leuven Medical School

Herestraat 49, bus 1021, B-3000 Leuven, Belgium

Email: peter.janssen@med.kuleuven.be

Abstract

Visual object information is necessary for grasping. In primates, the Anterior Intraparietal area (AIP) plays an essential role in visually-guided grasping. Neurons in AIP encode features of objects, but no study has systematically investigated the receptive field (RF) of AIP neurons. We mapped the RF of posterior AIP (pAIP) neurons in the central visual field using images of objects and small line fragments that evoked robust responses, together with less effective stimuli. The RF sizes we measured varied between 3 and 90 deg^2, with the highest response either at the fixation point or at parafoveal positions. A large fraction of pAIP neurons showed nonuniform RFs, with multiple local maxima in both ipsilateral and contralateral hemifields. Moreover, the RF profile could depend strongly on the

stimulus used to map the RF. Highly similar results were obtained with the smallest stimulus that evoked reliable responses (line fragments measuring 1-2 deg). The nonuniformity and dependence of the RF profile on the stimulus in pAIP was comparable to previous observations in the anterior part of the Lateral Intraparietal area (aLIP), but the average RF of pAIP neurons was located at the fovea whereas the average RF of aLIP neurons was located parafoveally. Thus, nonuniformity and stimulus-dependence of the RF may represent general RF properties of neurons in the dorsal visual stream involved in object analysis, which contrast markedly with those of neurons in the ventral visual stream.

Keywords: Receptive field, Anterior Intraparietal cortex, stimulus dependency.

Introduction

The visual system encodes object information to guide the hand during grasping (Castiello, 2005; Jeannerod et al., 1995). In the macaque monkey, the Anterior Intraparietal area (AIP) is part of the dorsal visual stream, which is known to be crucial for the visual analysis of space and the visual guidance of actions (Goodale and Milner, 1992). Reversible inactivation of AIP causes a pronounced grasping deficit (Gallese et al., 1994), and many AIP neurons are active during grasping, encoding both object features (Murata et al., 2000) and grip type (Baumann et al., 2009; Murata et al., 2000).

Previous studies (Murata et al., 2000; Sakata et al., 1998; Taira et al., 1990) have demonstrated that AIP contains a variety of neurons that either fire equally during grasping in the dark and in the light (motor-dominant neurons), less in the dark than in the light and during object fixation (visuomotor neurons), or only during grasping in the light and object fixation (visual dominant neurons). In recent years, it has become clear that AIP neurons not only respond to real-world objects but also to images of objects. Since Durand and colleagues showed stronger fMRI activations for disparity-defined curved surfaces compared to flat surfaces in AIP (Durand et al., 2007), subsequent studies have investigated

how AIP neurons encode 3D-shape defined by disparity at the single-cell level (Srivastava et al., 2009a). The 3D-shape representation in AIP appears fast (short latencies; 70ms) but relatively coarse (i.e. little sensitivity to small differences in disparity) and primarily based on the changes in disparity along the boundary of the stimulus (Theys et al., 2012). Moreover, these initial studies also observed a selectivity for the 2D contours of shapes in AIP. In agreement with this idea, we have shown that most neurons in the posterior subsector of AIP (pAIP) do not require the presence of binocular disparity, but exhibit robust selectivity to 2D images of familiar and unfamiliar objects presented on a display (Romero et al., 2012; Romero et al., 2013). Similar to the 3D domain, the selectivity for images of objects in pAIP was primarily based on the contours of the images, while surface information contributed very little to the neuronal selectivity. In a recent study (Romero et al., 2014) we reduced the outline shapes into small fragments, and observed that many pAIP neurons –even those that are active during object grasping– still fire strongly to very small line fragments measuring a mere 1–2 deg. Hence,the minimal effective shape features driving AIP neurons are remarkably simple.

A central concept in sensory neurophysiology is the receptive field (RF). Both in primary visual cortex (e.g. Hubel and Wiesel, 1968; Gilbert and Wiesel, 1992) and in extrastriate visual cortex (Op de Beeck and Vogels, 2000; Saito et al., 1986; Xiao et al., 1997), RF measurements constitute the very basic characterization that can be related to the neuronal computations in that area. However, despite the large number of investigations on the visual properties of AIP neurons, no study has systematically measured the RF of these cells. Both Srivastava et al. (Srivastava et al., 2009a) and Romero et al. (Romero et al., 2012) tested the responses of shape-selective pAIP neurons across a limited number of positions in the visual field, but firm conclusions about the RF organization in AIP could not be drawn from their studies –mainly due to the limited size of the area tested-. Detailed knowledge about the RF characteristics in pAIP is even more interesting given our previous finding that, for many of these pAIP neurons, the minimal effective shape feature can be a simple and very small line fragment, stimuli that

appear more suitable to activate neurons in early visual areas such as V2 (Ito and Komatsu, 2004) . The question, therefore, arises whether the RF size and structure of pAIP neurons is also similar to that of neurons in these early visual areas.

We mapped the RF of pAIP neurons using images of objects and contour fragments presented at 35 positions in the central visual field. The variety in RF size and structure we observed was remarkable, with some pAIP neurons only responding at a single position in the visual field (always the fovea) and others responding at every position tested. A sizeable fraction of pAIP neurons also exhibited highly nonuniform RFs with multiple local maxima interspersed with regions where no or weak responses were measured. In a subpopulation of pAIP neurons, the RF as determined with the preferred shape differed significantly from the RF as determined with the preferred outline fragment. These results provide the first detailed description of the RF organization of neurons in AIP.

Materials and Methods

Surgical and recording procedures

The experimental protocol was similar to that previously described elsewhere (Romero et al., 2014). Two male rhesus monkeys (Macaca mulatta; monkey H, 7 kg; monkey C, 6 kg) were trained to sit in a primate chair. Next, a head post (Crist Instruments) was implanted on the skull by using ceramic screws and dental acrylic. For this and all other surgical protocols, monkeys were kept under isoflurane anesthesia (1%) and strict aseptic conditions. All technical procedures were performed in accordance with the National Institute of Health's Guide for the Care and Use of Laboratory Animals, and approved by the Ethical Committee at the Katholieke Universiteit Leuven Medical School. Intensive training in passive fixation began after 6 weeks of recovery. Once the monkeys had acquired an adequate level of performance, a craniotomy was made, guided by anatomical magnetic resonance imaging (MRI)

(Horsley-Clark coordinates, 2P 12L) over the left hemisphere (Figure 1A). In order to confirm the recording positions, glass capillaries were filled with a 2% copper sulfate solution and inserted into a recording grid at 5 different locations while performing structural MRI (slice thickness, 0.6 mm). During the experiment, we recorded single-unit activity with tungsten microelectrodes (impedance: 1 MOhm at 1 kHz; FHC) inserted through the dura by means of a 23-gauge stainless-steel guide tube and a hydraulic microdrive (FHC). The neural activity was amplified and filtered between 300 and 5000 Hz. Spike discrimination was carried out on-line using a dual time window discriminator, and displayed with LabView and custom-built software. We monitored the right eye position by means of an infrared-based camera system (Eye Link II; SR Research) sampling the pupil position at 500 Hz. The stimuli were presented on a black background (luminance 8 cd/m2), using a monitor (Vision Research Graphics, resolution 1280x1024 pixels) equipped with a fast-decay P46-phosphor and operating at 120 Hz (viewing distance: 86 cm). A white square (covered with black tape to obscure it from view) was displayed in the lower right corner coinciding with the first video frame containing the stimulus and recorded with a photodiode. All recorded signals (eye position, neural activity, and photocell pulses) were digitized and processed at 20 kHz with a digital signal processor (DSP; C6000 series; Texas Instruments). The activity and silence transitions observed between the medial bank, the sulcus, and the lateral bank of the Intraparietal Sulcus (IPS), were useful to identify the target area. All neurons were recorded in the posterior part of area AIP (Figure 1A), within 7 (monkey H) and 9 mm (monkey C) from the tip of the IPS, consistent with previous studies in this region (Bauman et al., 2009; Lehman et al., 2013). In monkey H, we verified that no responses could be recorded during visually-guided saccades (see Romero et al., 2012). In monkey C, we obtained an anatomical MRI with the electrode in one of the recording positions (Romero et al., 2014).

Stimuli and tests

Our experimental paradigm consisted of a passive fixation task. Each trial began with the presentation of a small square in the center of the screen (fixation point; 0.2 x 0.2 deg). When the eye position remained within an electronically-defined 1 deg square window around the fixation point for at least 500 ms, a visual stimulus was presented on the screen, lasting for 500 ms. Trials were considered correct when the monkey kept a stable fixation until stimulus offset, receiving a drop of water as reward.

The *original stimulus set* used for the Search Test consisted of 21 two-dimensional (2D) surface area-equalized static images of natural and man-made objects, as illustrated in Figure 1B. Because of the large variation in surface area, we split the images into two categories (round vs elongated stimuli), and area-equalized the stimuli accordingly (surface area for round stimuli = 26.1 deg^2, diameter ~5 deg; surface area for elongated stimuli = 19.5 deg^2). The *fragments stimulus set* was created by resizing the images in the original stimulus set (surface area for round stimuli = 15.6 deg^2, diameter ~3 deg; surface area for elongated stimuli = 11.7 deg^2), removing the texture, and obtaining isolated fragments by the progressive segmentation of the resulting contours into 4, 8 and 16 different shape elements (Photoshop 8.0; Adobe; Figure 1C). The fragmentation was done manually in Photoshop along the main axes of the contour (outline). This set was used to determine the minimum effective shape feature evoking selectivity in AIP (see Romero et al., 2014 for more details). Because the surface area in the original contour was equalized within each stimulus category (round and elongated), the length of all fragments varied between stimuli (the size of the 4-fragment stimuli ranged from 3.8 to 5.1 deg, the size of the 8-fragment stimuli varied from 2.0 to 2.5 deg, and the size of the 16-fragment stimuli ranged between 1.0 to 1.3 deg).

During the experiments, we searched for responsive neurons in pAIP while the images of the original stimulus set (~5 deg diameter) were presented randomly interleaved on the display (*Search*

Test). For most neurons, the stimuli were presented at the fixation point (at the center of the display), but if no consistent responses were measured, we first mapped the RF (*Position Test*, Figure 1D), and repeated the Search Test while the images of the original stimulus set were presented at the RF center. If the neuron responded to at least one of the stimuli in our sample, we selected the object image evoking the strongest response (termed the *preferred* image) and a second object image to which the neuron did not respond or responded weakly (designated as the *nonpreferred* image). Both images were members of the same stimulus category (round or elongated), so that their surface area was equal. Next, a Position Test was used to obtain maps of the RF structure (area mapped: 12x8 deg around the fovea). For this test, the preferred and nonpreferred shapes were resized (~3 deg diameter), and presented interleaved at 35 different positions on the screen, spaced 2 deg apart, and covering both the ipsi-and contralateral visual hemifields (Figure 1D). Thus, the Position Test was composed of 70 conditions (2 stimuli presented at 35 positions), and we collected at least 6 trials (typically 10 trials) for each condition. We estimated the RF center separately for both shapes, comparing the online peristimulus-time histograms (PSTH) obtained at all positions. Third, we ran the *Reduction Test*, in which the contours obtained from the preferred and nonpreferred 3 deg images were presented together with their corresponding 4-, 8- and 16-fragments at the RF center. All fragments were shown at the location they occupied in the full contour stimulus. For a subset of cells, the preferred and nonpreferred fragments -obtained from the preferred outline- were next used to repeat the Position Test and remap the RF structure. With this procedure we were able to evaluate to what extent the RFs obtained in our pAIP neurons showed stimulus dependency. Finally, we used a *Retinotopy Test* to analyze wether the RFs of neurons in pAIP were retinotopic or object-centered. To do this, we compared the RFs obtained when the fixation point was presented at the center of the display and when the fixation point was presented at a location 5 deg in the ipsilateral hemifield (Figure 1D). For each cell, we chose the most effective stimulus (2D images or fragments). Due to the large number of stimuli used for the Position, Reduction

and Retinotopy tests, the fixation time and stimulus duration were reduced to 300 ms in these tasks (300 ms on/300 ms off).

Data analysis

All data analyses were performed in Matlab (Mathworks). The baseline firing rate was calculated from the mean activity recorded in the 300-ms interval preceding the stimulus onset. Net neural responses were then estimated by subtracting the baseline from the mean activity observed between 50 and 300 ms after the onset. For the Reduction Test, we computed an ANOVA to assess the significance of the fragment selectivity at each fragment level (4, 8 and 16-fragments). Following previous studies in the ventral stream (Tanaka et al., 1991), we designated the Minimum Effective Shape Feature (MESF) as the lowest level of fragmentation (4-, 8- or 16-fragment stimuli) for which we observed a response that was at least 70% of the response to the full contour (outline) and not significantly smaller than that response (one-sided t-test, $p > 0.05$; see Romero et al., 2014 and Tanaka et al., 1991). For the Position tests, contour plots were constructed by 2D linear interpolation of the mean responses to the preferred and the nonpreferred images or fragments. We categorized the RFs of the pAIP neurons we tested based on the net responses to the preferred object image (ANOVA), and the location and number of local maxima of the RF in the same test. To do this, we analyzed the significance of the response differences between different positions using ANOVA ($p < 0.05$). The RFs of neurons which did not show significant response differences across positions were labeled *large homogeneous*. For neurons with significant response differences across positions (i.e. confined RFs) we determined the global RF maximum and additional local maxima and minima with Matlab routines (Image toolbox, *imextendedmax* routine, threshold = 0.02). Neurons with significant response differences and a single global maximum were considered to have *uniform RFs*, either foveal or parafoveal depending on the location of the maximum response, and neurons with two or more maxima were considered to have *nonuniform RFs*. The size of the RF was determined by calculating the surface area (in deg^2) in the RF contour plots for which the normalized net

response (calculated by dividing each net response by the highest response in the test) was larger than 0.5, following previous RF studies in the ventral stream (Op De Beeck and Vogels, 2000). To quantify the correspondence between the RF as determined with different stimulus types, we calculated a 2D correlation coefficient between the RF obtained with the preferred and nonpreferred shapes, and between the RF determined with the preferred shape and the preferred fragment. Next, a two-way ANOVA with stimulus and position as factors was used to analyze whether the RF determined with the preferred shape differed significantly from the RF determined with the nonpreferred shape or the preferred fragment (interaction between the factors stimulus and position, $p < 0.05$).

In the Retinotopy Test, we first selected those neurons for which the center of the RF could be determined (ANOVA on net responses; $p < 0.05$), and calculated the shift of the RF center when the gaze was directed 5 deg away from the fixation point (center of the display) in the ipsilateral hemifield.

Results

We recorded the responses of 81 image-selective pAIP neurons to 2D images of objects presented at 35 positions in the visual field. We biased our recordings towards positions with strong visual responses, which makes difficult to estimate the fraction of image-selective neurons in pAIP (in a previous study, we observed selective responses in 79% of all responsive pAIP neurons; Romero et al., 2012). We first ran a Search Test on all neurons with the 21 different images used in previous studies (Romero et al., 2014). For all the neurons showing consistent responses and image selectivity in this test (N = 81), we selected the preferred and nonpreferred images to run the Position Test. A subpopulation of neurons (N = 58) was also studied with contour fragments (which had elicited selective responses in a Reduction Test; Romero et al., 2014), at the same 35 positions in the visual field.

Figure 2 illustrates the wide variety of RF profiles we observed in pAIP. The example neuron in Figure 2A responded selectively to the scissors presented at the fixation point, and did not respond to the image of a branch (t-test, $p < 0.001$). However, the image of the scissors did not evoke any significant response (t-test $p < 0.05$) at positions that were a mere 2 deg away from the fixation point, nor at more remote locations (ANOVA on the net responses to the preferred image, $p = 0.001$). Hence, the RF of this example neuron was very small (4.1 deg^2) and centered at the fixation point. In contrast, the RF of the example neuron in Figure 2B, when tested with the preferred image (banana), was larger (29.2 deg^2), and the maximal response was observed at a parafoveal position in the lower visual field (ANOVA on the net responses to the preferred image, $p = 0.001$). The RF of this second example neuron determined with the nonpreferred image (plant, RF size = 28.2 deg^2) was very similar to the RF as determined with the preferred image, except for a lower maximal response (Fig 2B, right panel). In both cases, the RF was confined (since significant response differences were measured across the 35 positions tested, ANOVA) and uniform: a single position in the visual field evoked a strong response and neighboring positions elicited progressively less (Figure 2B) or no response (Figure 2A).

The two previous example neurons illustrate that pAIP neurons can have confined RFs, either at the fovea or at parafoveal positions. However, we also observed neurons that responded over a large region of the central visual field. For example, the neuron in Figure 2C responded strongly to the image of a tangerine at virtually every position tested (RF size = 95.1 deg^2). The RF of this neuron was *large and homogeneous*, since no significant response differences were measured across the 35 positions tested (ANOVA, $p = 0.22$). The RF determined with the nonpreferred image was also extensive (86.8 deg^2) but nonuniform: the neuron responded more strongly to the image of the kong presented in the upper and lower contralateral hemifield, but less so at intermediate stimulus positions on the horizontal meridian (ANOVA on the average responses, $p = 0.008$). At least for this nonpreferred image, the RF contained two local maxima (see Materials and Methods).

The last two example neurons in Figure 2D and E illustrate even more clearly the complex RF profiles we observed in a subpopulation of pAIP neurons. The neuron in Figure 2D responded strongly to an image of a human hand (RF size= 77.7 deg^2) in the upper and contralateral visual field, but not in the ipsilateral hemifield (ANOVA on the response to the preferred image, $p = 0.002$). However, the RF of this example neuron had additional local maxima outside the global maximum. When tested with the nonpreferred image (tangerine), the neuron showed a smaller RF (32 deg^2) although localized in the same contralateral hemifield. Furthermore, the correspondence between the RF profiles as determined with the preferred and nonpreferred stimulus was relatively high (2D correlation = 0.76; two-way ANOVA, interaction between shape and position, $p = 0.587$; RF size for nonpreferred shape = 24 deg^2). The example neuron in Figure 2E represents an extreme case of a nonuniform RF profile with several local maxima, and a number of local minima located between the local maxima. The local minima we observed were not induced by random variability in response strength, since the differences between the responses at the local minima and those at the neighboring positions were significant (ANOVA on the net responses to the preferred image, $p =0.038$). Moreover, in some positions, the responses to the nonpreferred image were the opposite of the responses to the preferred image: for example, in the lower ipsilateral quadrant (2 deg down and 2 deg ipsilateral) the preferred image evoked weak responses whereas the nonpreferred image evoked the strongest response, compared to the lower contralateral quadrant (2 deg down and 4 deg contralateral) which evoked robust responses to the preferred image but very little responses to the nonpreferred image. The 2D correlation between the RF profiles was, therefore, low (2D correlation coefficient = 0.19; two-way ANOVA, interaction between shape and position, $p = 0.04$). The RF size for this cell was comparable for the two stimuli (RF size = 38.40 and 40.32 deg^2 when tested with the preferred and nonpreferred stimulus, respectively). Overall, the RFs in this pAIP region were extremely diverse in size (varying from 3.27 to 96.12 deg^2), location (foveal,

parafoveal or homogeneous), RF profile (uniform or nonuniform), and correspondence between different stimuli.

The example neurons in Figure 2 were all tested with images of objects measuring 3 deg. However, we recently showed that pAIP neurons frequently also respond to very small contour fragments measuring merely 1-2 deg (Romero et al., 2014). It might therefore be argued that the complex, nonuniform RF profiles we observed were related to the fact that these pAIP neurons respond mainly to small parts of the contour instead of the entire shape. Accordingly, we also determined the RF of 58 pAIP neurons with the most elementary stimulus to which the cell responded (by at least 70% of their maximal response). Figure 3 shows the RFs of the same neurons illustrated in Figure 2 tested with contour fragments. The example neuron in Figure 3A only responded to the image of the scissors at the fixation point (Figure 2A), and showed the same behavior when tested with the simplest shape feature to which the neuron responded (two parallel line fragments, Figure 3A). The 2D correlation coefficient between the RF determined with the intact image and the RF determined with the best fragment equaled 0.74 (two-way ANOVA, interaction between shape and position, $p = 0.623$). In contrast, the RF profile of the neuron illustrated in Figure 3B was very different when we used a small contour fragment compared to the intact object image (Figure 2B): although the region eliciting the highest response was located in the lower contralateral hemifield at a parafoveal position when tested with the intact image (both preferred and nonpreferred), this neuron responded best when the most effective contour fragment appeared in the upper contralateral quadrant (Figure 3B, left panel), and when a different fragment was used (right panel of Figure 3B), the neuron responded in the ipsi- and contralateral visual field. Hence, the 2D correlation coefficient between the preferred intact image RF and the preferred fragment RF was relatively low (0.22; two-way ANOVA, interaction between shape and position, $p = 0.127$). Neurons in pAIP with large RFs showed a similar range of correspondences between the intact image RF and the best fragment RF: the 2D correlation coefficient between the intact image RF and the

best fragment RF was higher for the neuron in Figure 2C and 3C (0.54 ; two-way ANOVA, interaction between shape and position, $p = 0.957$), but very low for the neurons illustrated in Figure 2D and 3D, and 2E and 3E (2D correlation coefficient = -0.18 and -0.12, respectively; two-way ANOVA, interaction between shape and position, $p = 0.002$ and 0.001). Overall, however, RF size did not correlate strongly with the correspondence between the best image RF and the best fragment RF ($r = 0.30$).

We verified the consistency of the RF profiles we measured by comparing the first half of the trials to the second half of the trials for each neuron tested in the Position Test. The example neurons in Figure 4A and D showed a very nonuniform RF (the cell in Figure 4A is the same as in Figure 2D), which was similar in both sets of trials (compare Figure 4B to Figure 4C, and Figure 4E to Figure 4F). The 2D correlation coefficient between the first half and the second half of the trials (preferred image) was 0.77 for the neuron in Figure 4B-C, and 0.81 for the neuron in Figure 4E-F. On average, the correspondence between the two sets of trials was relatively high (average 2D correlation coefficient = 0.68 for the preferred image and 0.54 for the nonpreferred image), which indicates that the complex RF profiles we observed were indeed reliable.

In our population of 81 pAIP neurons, 36 (44.4 %) showed large homogeneous RFs when tested with the preferred image (ANOVA on the net responses to the preferred image, $p > 0.05$), and 45 (55.6 %) showed confined RFs (ANOVA $p < 0.05$). In this latter group , 18 neurons (40%) exhibited a uniform RF with a single local maximum, mostly at the fovea (15/18), whereas the remaining 27 neurons (60%) showed nonuniform RFs, with 2 or more local maxima often extending into both the ipsi- and contralateral visual hemifields. Our classification of the RF types was based on the responses to the preferred image, but taking into account the responses to the nonpreferred shape did not alter the main results: only a very small subset of the neurons (4/81; 4.9%) showed a large homogeneous RF when determined with the preferred image, but a nonuniform RF when determined with the nonpreferred

image, similar to the example neuron in Figure 2D. Seven other neurons (7/81; 8.6%) showed the opposite behavior.

We calculated the mean RF for preferred and nonpreferred images by averaging the normalized responses of all 81 neurons tested (Figure 5A). Despite the large variability in RF sizes and profiles, the average RF was centered at the fixation point (average RF size for the preferred shape = 46.50 deg^2) and biased towards the contralateral hemifield. In a subset of the neurons (N=58), the RF was also measured using the fragments. In this subpopulation of pAIP neurons, the average RF determined with intact images (Figure 5B) was highly similar to that of the entire pAIP population. Although the selectivity for the fragments was less pronounced than for the images (compare left and right panels in Figure 5B and 5C), the overall location and RF profile for the fragments (RF size for the preferred fragment = 71.25 deg^2) was similar to the RF for the images of objects. Whereas the RF size as determined with fragments tended to be larger than the RF size as determined with images of objects, the average RF size did not significantly differ between the preferred image RF and the preferred fragment RF (t-test, $p = 0.483$; N=58). We also investigated where, in the visual field, pAIP neurons gave the strongest responses to the preferred object image (in view of the large number of cells with nonuniform RFs it is difficult to use the term 'RF center'). Figure 6 illustrates the number of neurons that gave the maximal response or a response statistically indistinguishable from the maximal response for each position in the visual field tested. The largest group of neurons (27/81, 33.3%) showed the highest response (or a response not significantly different from the highest response) at the fixation point. However, Figure 6 illustrates that many pAIP neurons also responded strongly at more eccentric positions. Furthermore, we observed a subtle contralateral bias in these RF center positions (as determined by the location of the global maximum: 29 RF centers were located in the contralateral hemifield and 24 in the ipsilateral hemifield ($p = 0.023$).

Figure 7 summarizes our findings by plotting the distributions of three basic RF parameters. The distribution of the RF size (median RF size = 42.9 deg^2) tested with the preferred shape (grey bars) and illustrated in Figure 7A shows two peaks: one for RFs between 31 and 40 deg^2, and a second one around 91-96 deg. Therefore, this distribution differed significantly from normal, both for the preferred (Jarque-Bera test for normality, $p = 0.02$) and the nonpreferred images (black bars, Jarque-Bera test for normality, $p = 0.01$). As can be expected, neurons with confined and nonuniform RFs comprised most of the first peak in the RF size distribution, whereas neurons with large homogeneous and nonuniform RFs formed the second peak in the distribution.

We quantified the uniformity of the RF by identifying the number of local maxima for all neurons with a confined RF (i.e. ANOVA $p < 0.05$, N=45). Although the RF of a subpopulation of pAIP neurons showed a single local maximum (i.e. uniform RFs: 18/45; 40%), a substantial fraction of these neurons (27/45: 60%) contained multiple local maxima (i.e. nonuniform RFs), and from those, a large fraction (21/45: 46.7%) showed 5 or more local maxima within the limited number of positions tested (Figure 7B). Moreover, some pAIP neurons (23% in monkey H and 32% in monkey C) also showed inhibitory responses (defined as a normalized response < - 0.15) at one or more positions tested. Since the median number of local maxima we observed equaled 3 (see Figure 7B), the presence of nonuniform RFs with multiple local maxima was not uncommon in pAIP. The correlation between the number of local maxima obtained in the RF test with 3 deg images (preferred image) and the number of local maxima obtained with fragments (preferred fragment) was 0.44 ($p = 0.001$), indicating a weak correspondence between the RF profile structure as determined with different stimuli.

In addition, we quantified the correspondence between the RFs determined with images of objects and contour fragments for the subpopulation of pAIP neurons tested with these different stimuli (N=58) by calculating the 2D correlation coefficient between the preferred image RF (preferred image) and the best

fragment RF (Figure 7C). The distribution of this 2D correlation coefficient did not differ significantly from unimodal (Hartigan's dip test, $p = 0.466$), but approximately one third of the population (N = 21; 36.2%) showed good correspondence between these two types of RFs (2D correlation coefficient > 0.5), whereas in almost half of the population this correspondence was poor or even absent (25/58, or 43.1% of the neurons showed a correlation of < 0.2). On average, the 2D correlation coefficient was low in both animals (0.29 in monkey H, and 0.35 in monkey C). Overall, 26 neurons (26/58: 44.8 %) showed a significant interaction between stimulus and position (two-way ANOVA, $p < 0.05$). For those cells that gave significant responses to the nonpreferred image, we also calculated the 2D correlation between the RF determined with the preferred images and the RF determined with the nonpreferred images (N = 64). As for the contour fragments, the average 2D correlation was low in both animals ($r = 0.31$ in monkey H and 0.45 in monkey C). Thus the RFs of AIP neurons can be highly nonuniform and frequently depend strongly on the stimulus used to map the RF.

To investigate the relation between RF uniformity and RF correspondence, we calculated the correlation between the degree of nonuniformity (the number of local maxima) and the RF correspondence (the 2D correlation coefficient calculated between the RF measured with the preferred image and the RF measured with the preferred fragment). Neurons with a higher number of local maxima tended to show less correspondence between the RF measured with images and the RF measured with fragments ($r = -0.33$; $p = 0.01$). We also investigated whether the differences in the RF determined with the preferred and nonpreferred shape were associated with particular regions in the visual field. To that end, we plotted the difference in the neural response to the preferred and nonpreferred shape for all neurons with a nonuniform RF (N = 27). Figure 8 demonstrates that the largest response differences between the preferred and the nonpreferred shape were observed around the fixation point.

The marked nonuniformity of the RFs we observed might suggest that the RFs in pAIP were not retinotopic anymore but rather object- or world-centered. To test this possibility, we mapped the RF of 59 pAIP neurons for two directions of gaze: towards the center of the display and in a direction 5 deg to the ipsilateral hemifield. The example neuron in Figure 9A had a well-defined parafoveal RF, for which the maximal response was measured at a position 2 deg from the central position in the lower visual field on the vertical meridian. When the monkey fixated a spot 5 deg to the left, the RF shifted together with the shift in gaze (by 4 deg), so that the maximal response of the neuron was again measured close to the fixation point, consistent with a retinotopic RF. When tested with the line fragments, the horizontal shift in the position of the RF center was even more obvious (Figure 9B). Calculating the shift of the RF based on the contours instead of the global maximum did not change the main results (data not shown).

Similar to the data obtained in the Position Test, we verified the consistency of the observed shifts in the RF by comparing the first half of the trials to the second half of the trials in which the monkey fixated in a direction 5 deg to the ipsilateral hemifield. Figure 9C and D illustrate that the shifts in the RF were indeed reliable. For the example neuron, the 2D correlation coefficient between the two sets of trials was 0.84 for the preferred and nonpreferred images, respectively, and 0.71 and 0.89 for the preferred and nonpreferred fragments, respectively. On average, the two sets of trials correlated strongly (mean 2D correlation coefficient = 0.78 for the preferred image, and 0.74 for the preferred fragment).

We plotted the distribution of the shifts in either the horizontal, the vertical or the diagonal direction of the RF center (global maximum) for all 59 neurons tested (Figure 9E). The median shift in the location of the RF center was 4 deg, indicating that most RFs in pAIP are indeed retinotopic. Even the subpopulation of neurons with a nonuniform RF (i.e. two or more local maxima, N = 27) tended to shift

the position of the RF maximum by 4.3 deg on average. Consistent with these observations, the mean 2D correlation between the RF determined with the two directions of gaze was very low (2D correlation = 0.03 for the preferred image and 0.08 for the nonpreferred image). We also verified that the observed shifts were not simply due to noise in the data by calculating the shifts of the RF based on a test-retest procedure (first half of the trials vs second half of the trials) for the condition in which the fixation point appeared in the center of the display, and compared the distribution of these shifts with the observed shifts. As expected, the distribution of the test-retest shifts was centered at zero, and differed significantly from the observed distribution of shifts (Kolmogorov-Smirnov test, $p < 0.001$).

To better illustrate the nature of the pAIP RFs, we plotted the observed number of global maxima at each position tested when the animal fixated a spot that appeared 5 deg to the left, together with the predicted number of global maxima (based on the data when the animal fixated a spot in the center of the display) according to the two reference frames, spatiotopic (Figure 10A) and retinotopic (Figure 10B). Clearly, the retinotopic reference frame matches our observations much better than the spatiotopic reference frame.

Discussion

We mapped the RF of pAIP neurons responding to images of objects and fragments of object contours presented in the central visual field. The range of RF sizes and profiles was remarkably large in pAIP. The RF center was frequently located at the fixation point, but many pAIP neurons responded maximally at parafoveal positions. Although some pAIP RFs appeared largely homogeneous, we also observed nonuniform RFs with multiple local maxima. Finally, the RF plotted with an object image differed frequently from the RF as determined with a contour fragment.

We tested a limited number of positions covering the central 8 (vertical) by 12 (horizontal) deg of the visual field. The largest eccentricity tested in this study equaled 11 deg along the horizontal meridian

in the contralateral visual field in the Retinotopy Test. Therefore, our conclusions can only pertain to the RF characteristics of pAIP neurons in the central visual field, and we cannot determine how far eccentric the RFs of these pAIP neurons extend. However, it is highly unlikely that our main observations (range of RF sizes, nonuniformity of many RFs, dependence of the RF profile on the stimulus) would have been substantially different if we would have tested a larger range of eccentricities.

The cornerstone of sensory neurophysiology remains charting the RF of sensory neurons (Schwartz et al., 2006; Wu et al., 2006). Despite a growing interest in both the macaque AIP (Murata et al., 2000; Srivastava et al., 2009a; Theys et al., 2012; Verhoef et al., 2010) and its (putative) human homologue phAIP (Culham and Valyear, 2006; Durand et al., 2009; Grefkes et al., 2002; Orban, 2011; Srivastava et al., 2009a), a systematic study of the RF properties of AIP neurons was still lacking. Since it is not straightforward to map the RF of neurons that are only active during grasping of real-world objects, we capitalized on the finding that pAIP neurons respond selectively to images of objects presented on a display (Romero et al., 2012). The study by Romero et al. (Romero et al., 2012) observed that pAIP neurons can have either foveal or parafoveal RFs, but the limited number of positions tested prevented to draw firm conclusions about the RF extent and profile in pAIP. More recently, we investigated which aspect of the shape contour is driving the AIP responses using a stimulus reduction approach (Romero et al., 2014). For most pAIP neurons, the minimal effective shape feature consisted of very small line fragments measuring a mere 1–2 deg. Note that a number of pAIP neurons in this study (N =12) was also strongly active during object grasping, as described in more detail in our previous study (Romero et al., 2014). The RFs of these neurons were highly similar to those of the other pAIP neurons in this study.

Recent studies have investigated the functional and anatomical properties of neurons in pAIP (Premereur et al., 2015; Van Dromme et al., 2015), and have compared them to those of neurons in neighboring area LIP. The large fMRI activation in the anterior lateral IPS related to sensitivity for the

disparity-defined depth structure of objects consists of two patches, one in aAIP and one in pAIP (Van Dromme et al., 2015), while the spatially-selective saccadic activity typical of area LIP is located posterior from pAIP. Moreover, using electrical microstimulation of those patches during fMRI (EM-fMRI), (Premereur et al., 2015) showed that the effective connectivity of pAIP differed markedly from that of aAIP and LIP: while aAIP was connected to a somatomotor network including F5, PFG, and SII, pAIP was connected to ventral stream areas TE and TEO, and the LIP site to area FST. Note that monkey C in our study was also used in the EM-fMRI study of (Premereur et al., 2015), and that the effective connectivity of our recording site was highly similar to the pAIP sites of the other two animals in that study. Thus, in view of the presence of depth structure selectivity (Srivastava et al., 2009b; Van Dromme et al., 2015), grasping activity (Romero et al., 2014; Theys et al., 2013), the absence of saccadic responses and its distinct anatomical connectivity, our recording area corresponds functionally much more to AIP. Note that the earliest investigations in AIP using grasping tasks also included a large sector of the anterior IPS extending into the anatomically defined LIP (Sakata et al., 1995), consistent with our data and those of previous studies.

An alternative view may be that our recording area simply represents the part of LIP that is involved in making small saccadic eye movements. At least some of our RF data argue against this alternative view. Almost two-thirds of the neurons we recorded had either large homogeneous RFs (44%) or small foveal RFs (19%), both of which cannot result in spatially-selective saccadic activity. Moreover, the example neuron with a foveal RF shows that a displacement of the optimal stimulus (a line fragment measuring 1.5 deg) by a mere 2 deg reduced the response to baseline levels. If such a neuron would encode small saccades, the saccade amplitudes would have to be less than 2 deg. Obviously, the boundaries between cortical areas can be difficult to delineate as considerable overlap in functional properties may exist, but the functional characterization based on task-related activity (grasping vs saccades) seems highly appropriate to distinguish AIP from LIP.

Several RF characteristics we observed were quite unexpected for an area of the dorsal visual stream. For example, a sizeable proportion of pAIP neurons only responded at the fovea and failed to respond when the preferred stimulus was presented a mere 2 deg from the fovea, even when tested with small line fragments. A second striking RF feature was the strong nonuniformity of the RF of many pAIP neurons, with several local maxima interspersed with positions that evoked no or much less response. Furthermore, the RF determined with images of intact objects frequently differed substantially from the RF determined with line fragments, and different shapes could give rise to very different RF profiles. Despite the RF nonuniformity and the strong dependence on the stimulus used to map the RF, we found that the RFs in pAIP were predominantly retinotopic, consistent with a previous study (Lehmann and Scherberger, 2013).

These RF characteristics in pAIP bared resemblance to those measured in neighboring area anterior LIP (aLIP; Janssen et al., 2008), in which the RFs were determined using simple shapes (squares, triangles) and visually-guided saccades. In both regions the RFs can be nonuniform with multiple local maxima, and in both regions the RF profile can depend on the stimulus used to map the RF, as may also be the case in the Ventral Intraparietal area (VIP; Chen et al., 2014). In aLIP, the RF profile also depended on the task used (passive fixation or saccades; Janssen et al., 2008). In fact, a dependence of the RF on the task used may be a general property of neurons in the dorsal visual stream (Ben Hamed et al., 2002; Womelsdorf et al., 2008). The main difference between pAIP and aLIP is therefore the location of the RF center: in pAIP most RFs are centered on the fovea, whereas in aLIP the average RF center was eccentric, approximately 5 deg from the fovea. Since pAIP and aLIP are adjacent to each other, it is difficult to distinguish between the two areas with RF mapping alone. Ben Hamed and colleagues (Ben Hamed et al., 2001) previously mapped the RFs of neurons in the lateral bank of the IPS, in a region that must have comprised both LIP and a sizeable part of AIP. In that study, the more dorsal and anterior recording sector contained more central RFs, the more ventral anterior sector was dominated by lower visual field

RFs, and the more posterior sector contained upper visual field RFs. Hence, although we did not have a sufficient number of recording sites to investigate the topographical organization of this region, the possibility exists that our pAIP recordings were located more dorsally in the lateral bank of the IPS, and the previous aLIP recordings (Janssen et al., 2008), more ventrally. Functionally, however, most studies have delineated AIP based on the responses during grasping and the absence of saccadic activity (Gallese et al., 1994; Murata et al., 2000; Taira et al., 1990), which we also observed in our pAIP recording sites (Romero et al., 2014). The functional criterion (grasping vs saccades) roughly corresponds to RF location, since many grasping neurons in pAIP are visual-dominant (Baumann et al., 2009), responding to the visual presentation of the object which is typically foveated during grasping (Johansson et al., 2001), and saccade neurons possess eccentric RFs. Note that fMRI studies in macaques have also identified a central visual field representation in the lateral bank of the IPS (Arcaro et al., 2011). Many AIP neurons respond when the animal executes a grasping action and also when the animal observes a video of the same action (Pani et al., 2014), i.e. mirror-like activity. Most AIP neurons with mirror-like activity are also activated by a simple shape moving in the visual field. To a large extent, these responses are driven by visual information about the presence of a hand (or another object) near the object to be grasped at the fixation point (Pani and Janssen, unpublished observations). Hence, the predominance of foveal information explains why we did not observe a lower visual field dominance in our RF mapping experiment (the own hand moves in the lower visual field towards the object): even pAIP neurons that become active when the hand starts to move towards the object (so-called non-object type visuomotor neurons) respond mostly to visual stimulation at or near the fovea. The presence of foveal and retinotopic RFs has also been documented in the dorsal sector of area V6A (Galletti et al., 1999; Gamberini et al., 2011), part of the dorsomedial visual stream and anatomically connected to AIP (Gamberini et al., 2009). Moreover, V6A neurons also encode grip types (Fattori et al., 2010) and objects (Fattori et al., 2012), similar to AIP (Baumann et al., 2009).

How can a detailed description of the RF help to understand the role of pAIP neurons during visually-guided grasping? In our study, a large fraction of pAIP neurons (38%) responded maximally at the fixation point or at positions adjacent to the fixation point. Given the size of the stimuli we used to map the RF (3 deg) and the observation that most pAIP neurons respond to the contour of the shape, the shape features driving the response appeared very close to the fixation point when the shape was presented at one of the positions adjacent to the fixation point, which can therefore also be considered foveal. Obviously, the strong link between gaze direction and grasping point (Johansson et al., 2001) suggests that AIP neurons with foveal RFs may play a role in the visual analysis of the object (or object part) before it is grasped. It may be more difficult to provide a functional interpretation of neurons with nonuniform RFs. Such neurons appear to possess multiple excitatory and inhibitory (or less responsive) regions within their RF, but this RF structure may be stimulus-dependent. In our previous study (Romero et al., 2014), we observed that the preference of AIP neurons for small line fragments tested at one position is radically different when we presented the same fragments at a different position a mere 2.5 deg away from the first position. Thus, AIP neurons may not simply signal the presence of its preferred contour fragment (or shape) in its RF, but always the combination of a contour fragment at a particular position in the RF. Similar to neighboring area LIP then (Janssen et al., 2008), neurons in the IPS may not provide an abstract representation of object shape, but rather signal a combination of a shape (feature) and position in the visual field. In contrast to the ventral stream, which achieves selectivity and invariance of the shape preference across transformations such as size, position and visual cue (DiCarlo et al., 2012), the action-oriented dorsal stream may never discount position because actions are always executed in space. Thus our results suggest that the RF of sensory neurons may have a different status in high-level visuomotor areas such as AIP compared to early or ventral stream visual areas.

Acknowledgements: We thank Sara De Pril, Astrid Hermans, Piet Kayenbergh, Gerrit Meulemans, Stijn Verstraeten, Marc Depaep, Wouter Depuydt and Inez Puttemans for technical assistance.

Grants: This work was supported by Fonds voor Wetenschappelijk Onderzoek Vlaanderen grants (G.0495.05, G.0713.09), Programmafinanciering (PFV/10/008), IUAP VII-11 and ERC-2010-StG-260607.

Disclosures: The authors declare no conflicts of interest.

Reference List

Arcaro MJ, Pinsk MA, Li X, Kastner S (2011) Visuotopic organization of macaque posterior parietal cortex: a functional magnetic resonance imaging study. J Neurosci 31:2064-2078.

Baumann MA, Fluet MC, Scherberger H (2009) Context-specific grasp movement representation in the macaque anterior intraparietal area. J Neurosci 29:6436-6448.

Ben Hamed S, Duhamel JR, Bremmer F, Graf W (2001) Representation of the visual field in the lateral intraparietal area of macaque monkeys: a quantitative receptive field analysis. Exp Brain Res 140:127-144.

Ben Hamed S, Duhamel JR, Bremmer F, Graf W (2002) Visual receptive field modulation in the lateral intraparietal area during attentive fixation and free gaze. Cereb Cortex, 12: 234-245.

Castiello U (2005) The neuroscience of grasping. Nat Rev Neurosci 6:726-736.

Chen X, DeAngelis GC, Angelaki DE (2014) Eye-centered visual receptive fields in the ventral intraparietal area. J Neurophysiol 112:353-361.

Culham JC, Valyear KF (2006) Human parietal cortex in action. Curr Opin Neurobiol 16:205-212.

DiCarlo JJ, Zoccolan D, Rust NC (2012) How does the brain solve visual object recognition? Neuron 73:415-434.

Durand JB, Nelissen K, Joly O, Wardak C, Todd JT, Norman JF, Janssen P, Vanduffel W, Orban GA (2007) Anterior regions of monkey parietal cortex process visual 3D shape. Neuron 55:493-505.

Durand JB, Peeters R, Norman JF, Todd JT, Orban GA (2009) Parietal regions processing visual 3D shape extracted from disparity. Neuroimage 46:1114-1126.

Fattori P, Breveglieri R, Raos V, Bosco A, Galletti C (2012) Vision for action in the macaque medial posterior parietal cortex. *J Neurosci* 32: 3221-3224.

Fattori P, Raos V, Breveglieri R, Bosco A, Marzocchi N, Galletti (2010) The dorsomedial pathway is not just for reaching: grasping neurons in the medial parieto-occipital cortex of the macaque monkey. *J Neurosci* 30:342-349.

Gallese V, Murata A, Kaseda M, Niki N, Sakata H (1994) Deficit of hand preshaping after muscimol injection in monkey parietal cortex. Neuroreport 5:1525-1529.

Galletti C, Fattori P, Kutz DF, Gamberini M (1999) Brain location and visual topography of cortical area V6A in the macaque monkey. Eur J Neurosci 11: 575-582.

Gamberini M, Galletti C, Bosco A, Breveglieri R, Fattori P (2011). Is the medial posterior parietal area V6A a single functional area? J Neurosci 31: 5145-5157.

Gamberini M, Passarelli L, Fattori P, Zucchelli M, Bakola S, Luppino G, Galletti C (2009) Cortical connections of the visuomotor parietooccipital area V6Ad of the macaque monkey. J Comp Neurol 513:622-642.

Gilbert CD, Wiesel TN (1992) Receptive field dynamics in adult primary visual cortex. Nature 356: 150-152.

Goodale MA, Milner AD (1992) Separate visual pathways for perception and action. Trends Neurosci 15:20-25.

Grefkes C, Weiss PH, Zilles K, Fink GR (2002) Crossmodal processing of object features in human anterior intraparietal cortex: an fMRI study implies equivalencies between humans and monkeys. Neuron 35:173-184.

Hubel DH, Wiesel TN (1968) Receptive fields and functional architecture of monkey striate cortex. J Physiol 195:215-243.

Ito M, Komatsu H (2004) Representation of angles embeded within contour stimuli in area V2 of macaque monkeys. J Neurosci 24:3313-3324.

Janssen P, Srivastava S, Ombelet S, Orban GA (2008) Coding of shape and position in macaque lateral intraparietal area. J Neurosci 28:6679-6690.

Jeannerod M, Arbib MA, Rizzolatti G, Sakata H (1995) Grasping objects: the cortical mechanisms of visuomotor transformation. Trends Neurosci 18:314-320.

Johansson RS, Westling G, Backstrom A, Flanagan JR (2001) Eye-hand coordination in object manipulation. J Neurosci 21:6917-6932.

Lehmann SJ, Scherberger H (2013) Reach and gaze representations in macaque parietal and premotor grasp areas. J Neurosci 33:7038-7049.

Murata A, Gallese V, Luppino G, Kaseda M, Sakata H (2000) Selectivity for the shape, size, and orientation of objects for grasping in neurons of monkey parietal area AIP. J Neurophysiol 83:2580-2601.

Op de Beeck H, Vogels R (2000) Spatial sensitivity of macaque inferior temporal neurons. J Comp Neurol 426:505-518.

Orban GA (2011) The extraction of 3D shape in the visual system of human and nonhuman primates. Annu Rev Neurosci 34:361-388.

Pani P, Theys T, Romero MC, Janssen P (2014) Grasping execution and grasping observation activity of single neurons in the macaque Anterior Intraparietal area. J Cogn Neurosci. 26: 2342-2355.

Premereur E, Van Dromme IC, Romero MC, Vanduffel W, Janssen P (2015) Effective connectivity of depth-structure-selective patches in the lateral bank of the macaque intraparietal sulcus. PLoS Biol 13:e1002072.

Romero MC, Pani P, Janssen P (2014) Coding of shape features in the macaque anterior intraparietal area. J Neurosci 34:4006-4021.

Romero MC, Van Dromme IC, Janssen P (2013) The role of binocular disparity in stereoscopic images of objects in the macaque anterior intraparietal area. PLoS One 8:e55340.

Romero MC, Van D, I, Janssen P (2012) Responses to two-dimensional shapes in the macaque anterior intraparietal area. Eur J Neurosci 36:2324-2334.

Saito H, Yukie M, Tanaka K, Hikosaka K, Fukada Y, Iwai E (1986) Integration of direction signals of image motion in the superior temporal sulcus of the macaque monkey. J Neurosci 6:145-157.

Sakata H, Taira M, Kusunoki M, Murata A, Tanaka Y, Tsutsui K (1998) Neural coding of 3D features of objects for hand action in the parietal cortex of the monkey. Philos Trans R Soc Lond B Biol Sci 353:1363-1373.

Sakata H, Taira M, Murata A, Mine S (1995) Neural mechanisms of visual guidance of hand action in the parietal cortex of the monkey. Cereb Cortex 5:429-438.

Schwartz O, Pillow JW, Rust NC, Simoncelli EP (2006) Spike-triggered neural characterization. J Vis 6: 484–507.

Srivastava S, Orban GA, De Maziere PA, Janssen P (2009a) A distinct representation of three-dimensional shape in macaque anterior intraparietal area: fast, metric, and coarse. J Neurosci 29:10613-10626.

Srivastava S, Orban GA, De Maziere PA, Janssen P (2009b) A distinct representation of three-dimensional shape in macaque anterior intraparietal area: fast, metric, and coarse. J Neurosci 29:10613-10626.

Taira M, Mine S, Georgopoulos AP, Murata A, Sakata H (1990) Parietal cortex neurons of the monkey related to the visual guidance of hand movement. Exp Brain Res 83:29-36.

Tanaka K, Saito H, Fukada Y, Moriya M (1991) Coding visual images of objects in the inferotemporal cortex of the macaque monkey. *J Neurophysiol* 66: 170-189.

Theys T, Pani P, van LJ, Goffin J, Janssen P (2013) Three-dimensional shape coding in grasping circuits: a comparison between the anterior intraparietal area and ventral premotor area F5a. J Cogn Neurosci 25:352-364.

Theys T, Srivastava S, van LJ, Goffin J, Janssen P (2012) Selectivity for three-dimensional contours and surfaces in the anterior intraparietal area. J Neurophysiol 107:995-1008.

Van Dromme IC, Vanduffel W, Janssen P (2015) The relation between functional magnetic resonance imaging activations and single-cell selectivity in the macaque intraparietal sulcus. Neuroimage 113:86-100.

Verhoef BE, Vogels R, Janssen P (2010) Contribution of inferior temporal and posterior parietal activity to three-dimensional shape perception. Curr Biol 20:909-913.

Womelsdorf T, Anton-Erxleben K, Treue S (2008) Receptive field shift and shrinkage in macaque middle temporal area through attentional gain modulation. J Neurosci 28:8934-8944.

Xiao DK, Raiguel S, Marcar V, Orban GA (1997) The spatial distribution of the antagonistic surround of MT/V5 neurons. Cereb Cortex 7:662-677.

Wu MC, David SV, Gallant JL (2006) Complete functional characterization of sensory Neurons by system identification. *Annu Rev Neurosci* 29: 477–505.

Figure Captions

Figure 1. Methods. (A) Anatomical magnetic resonance image and lateral view of the macaque brain, indicating the reconstructed recording positions in pAIP. Inside the dashed square, detail of the coronal section showing the microelectrode inserted into one of the recording positions. (B) Stimuli in the Search Test. (C) Reduction Test. Example of the fragmentation performed on one of the stimuli (scissors). After extracting the outline of the image, we segmented the contour into, 4, 8 and 16 different fragments in order to determine the minimum effective feature evoking selectivity.(D) Position and Retinotopy tests. Images of objects and fragments were presented at each node of the grid and used to map the RF (area mapped: 12x8 deg around the fovea; 35 positions). In the Retinotopy Test, the fixation point was presented at the center of the display and at 5 deg in the ipsilateral hemifield.

Figure 2. Example neurons in the Position Test (3 deg images). The graphs are 2D-interpolated maps of the average responses to the preferred (left) and nonpreferred images (right) when tested with the 3 deg images of objects. The colors indicate the strength of the neural response (varying between 0 and the maximum response of the cell). The intersections on the grid lines indicate each of the 35 positions tested, where [0,0] is the central position (at the fixation point), and +6 deg azimuth is contralateral. Red circles indicate positions with a significant ($p < 0.01$, t-test) response to the stimulus. Note the actual area of the visual field was larger than that illustrated in the figure because of the size of the images used (3 deg).This figure summarizes the three main RF profiles observed in pAIP. (A,B) The example neurons in these panels show a uniform RF profile, exhibiting one unique local maxima either at the fovea (in A) or at 2 deg eccentricity (in B). (C) Example of a pAIP neuron with a large homogenous RF profile. (D,E) pAIP neurons showing a nonuniform RF, with multiple local maxima for both the preferred and nonpreferred images.

Figure 3. Example neurons in the Position Test with fragments. Interpolated maps showing the same neurons of Figure 2 but now tested with the preferred (left) and nonpreferred fragment (right) as determined in the Reduction Test. (A) Example cell that preserved the RF structure across stimulus types. (B) Example cell showing a more nonuniform profile when tested with the fragments. (C) pAIP neuron with a large homogenous RF profile. (D,E) Example neurons showing nonuniform RFs, with multiple local maxima obtained for both the 3 deg and the fragment stimuli. Same conventions as in Figure 2.

Figure 4. Analysis of the test-retest consistency in our pAIP population. (A) Example cell with a nonuniform RF, the same as in Figure 2D. (B,C) RF profile of the same neuron when using the first (B) and the second (C) half of the trials. The 2D correlation coefficient between the two data sets was 0.77 for preferred and 0.61 for the nonpreferred image. (D-F) Second example cell showing highly correlated

RF profiles in the test-retest analysis (2D correlation coefficient = 0.81 for the preferred and 0.79 for the nonpreferred image). Conventions are the same as in Figures 2 and 3.

Figure 5. Average receptive field. (A) Average normalized response of all neurons in our pAIP population (N=81) when tested in the Position Test with the preferred and nonpreferred 3 deg image. (B) Average normalized response to the same preferred and nonpreferred 3 deg image for the subpopulation of pAIP neurons tested with fragments (N=58). (C) Average normalized response of the subpopulation of pAIP neurons tested with the preferred and nonpreferred fragment (N=58). Conventions are the same as in figures 2-4.

Figure 6. Spatial distribution of the pAIP RFs. The intersections on the grid lines indicate the 35 positions tested in the Position Test. The number of neurons showing their maximal response (global maxima) or a response statistically indistinguishable from the maximal response at each particular position is indicated by the radius of the grey circles.

Figure 7. Population analysis (A) Histogram of RF size tested with the preferred (grey bars) and nonpreferred (black bars) 3 deg stimuli. (B) Histogram of the number of local maxima when tested with the preferred (grey bars) and nonpreferred (black bars) 3 deg images. (C) Distribution of the 2D correlations between the RF tested with the preferred 3 deg images and the RF tested with the preferred fragment across our population of pAIP neurons.

Figure 8. Average difference (in spikes/sec) between the RF map measured with the preferred image and the RF map measured with the nonpreferred shape, for all neurons with a nonuniform RF (N = 27). Same conventions as in previous figures.

Figure 9. Retinotopy Test. (A) Example neuron with a uniform RF profile when tested with a 3 deg image (left panel: preferred image; right panel: nonpreferred image). The global maximum of the RF is

displaced into the ipsilateral hemifield when the fixation point is moved 5 deg ipsilaterally from the center. (B) The same shift in the RF center is observed when the neuron is tested with 1 deg fragments. (C-D) Analysis of the test-retest consistency by comparing the first and the second half of the trials collected for this neuron when the monkey fixated in a direction 5 deg to the ipsilateral hemifield. The same analysis was repeated for the cell responses obtained with 3 deg images (C) and fragments (D). (E) Distribution of the estimated distance between the RF centers obtained in the Position and the Retinotopy tests for the same population of pAIP neurons (N = 59). Same conventions as in Figure 2.

Figure 10. Graphic comparison of the spatiotopic or retinotopic behavior of neurons in our pAIP population. Yellow circles indicate the number of neurons with a global maximum at that position when the animal fixated a spot that appeared 5 deg to the left, whereas blue circles indicate the predicted number of neurons, according to a spatiotopic (A) or a retinotopic (B) reference frame. As for figure 6, the intersections on the grid lines indicate the 35 positions tested in the Position Test.

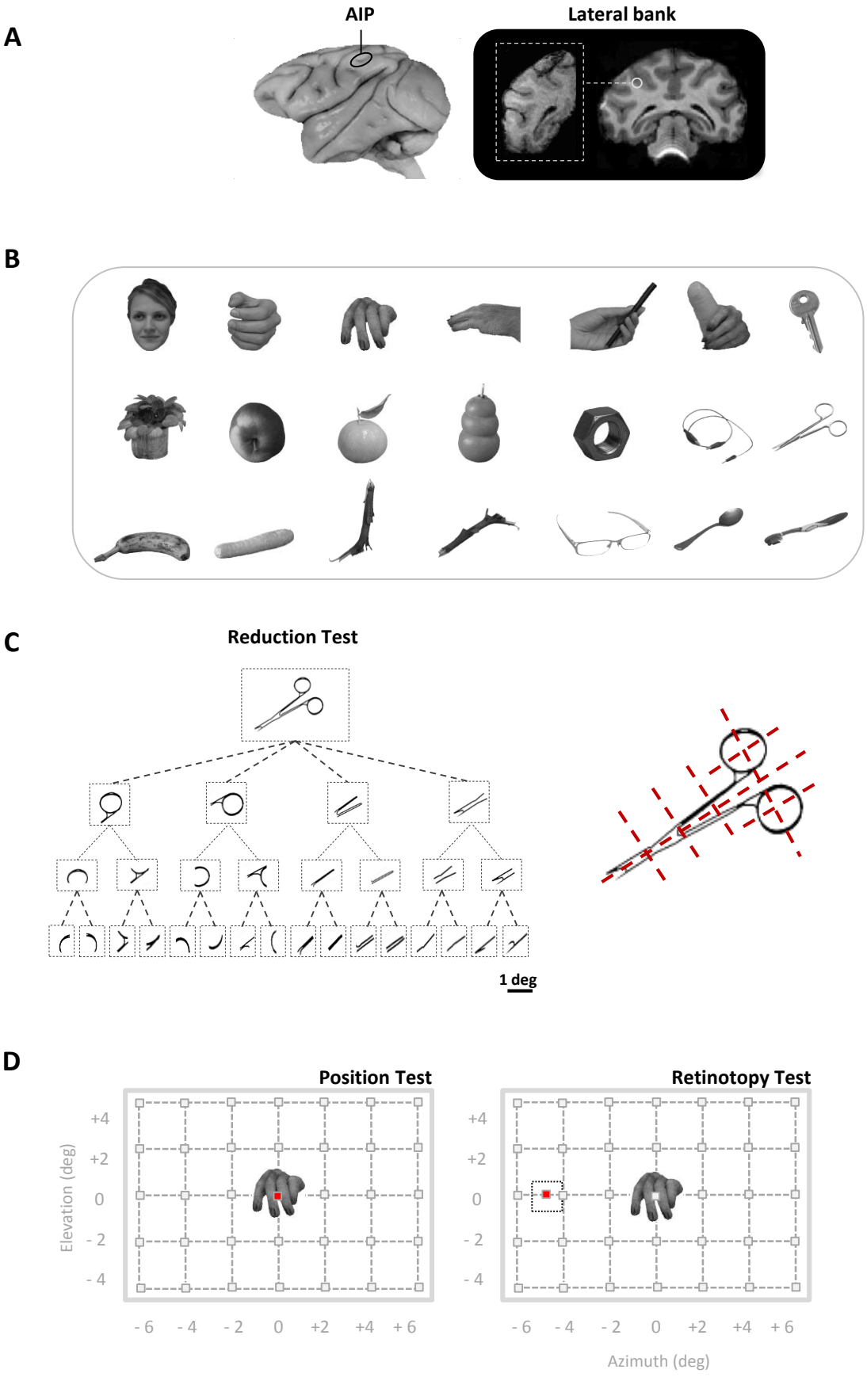
A
AIP
Lateral bank
B
C
Reduction Test
1 deg
D
Position Test
Retinotopy Test
Elevation (deg)
+4
+2
0
- 2
- 4
- 6
- 4
- 2
0
+2
+4
+ 6
Azimuth (deg)

Figure 1

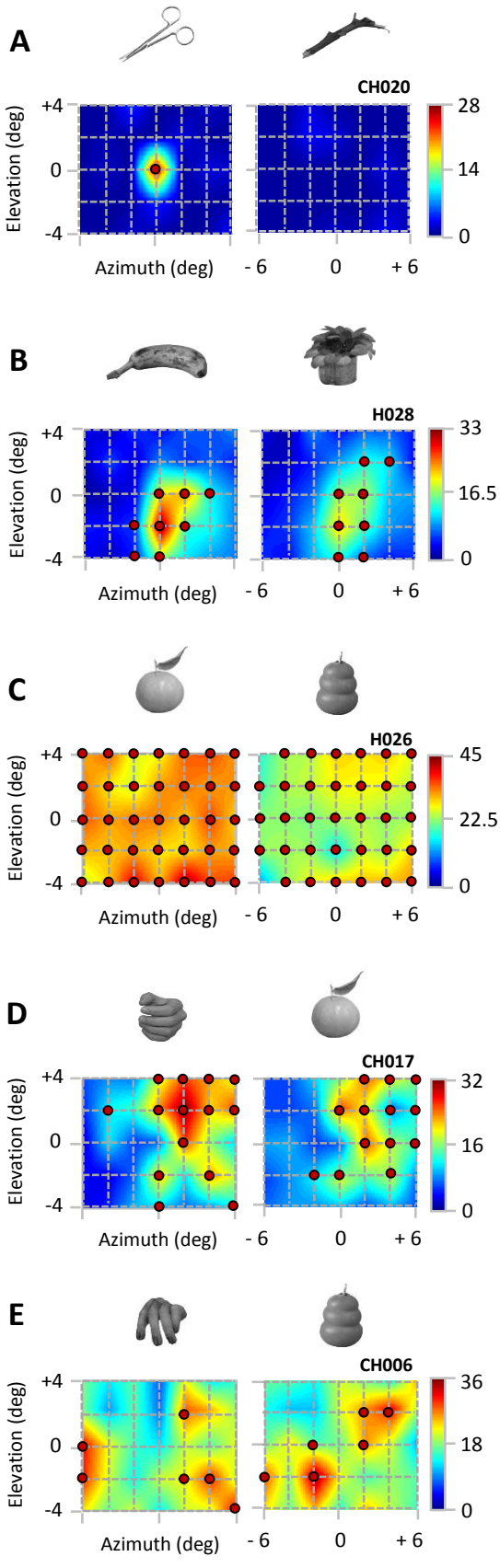
A
CH020
+4
0
-4
Elevation (deg)
28
14
0
Azimuth (deg)
- 6
0
+ 6
B
H028
33
16.5
0
C
H026
45
22.5
D
CH017
32
16
E
CH006
36
18

Figure 2

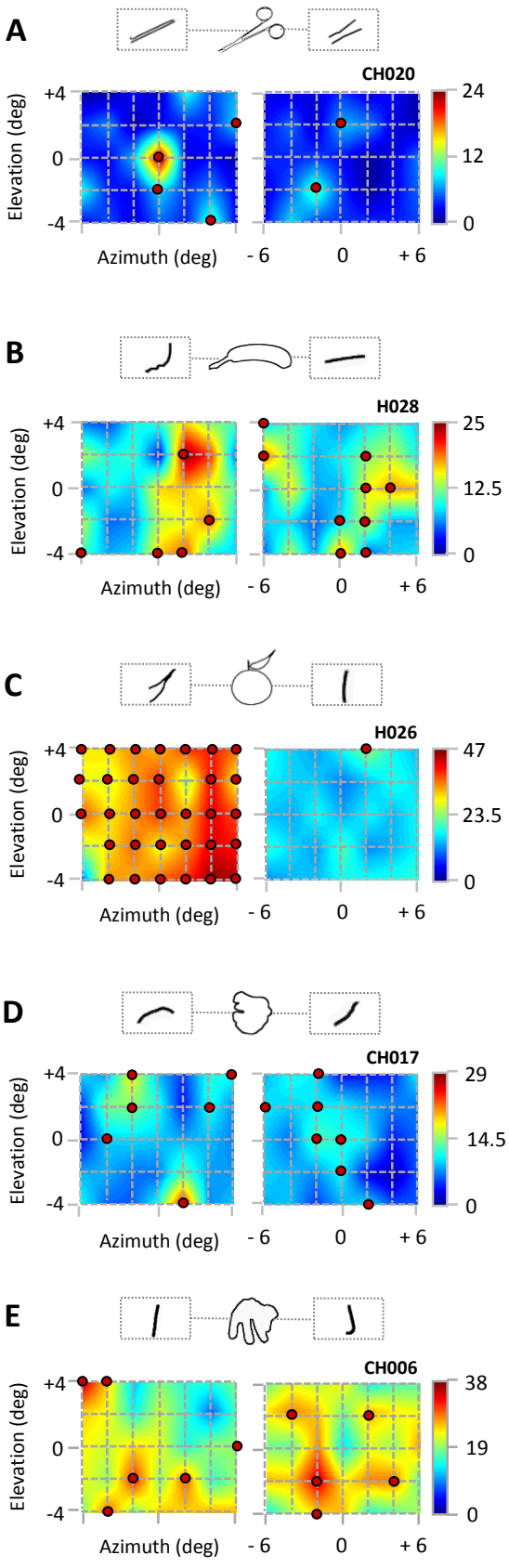
A
CH020
+4
0
-4
Elevation (deg)
Azimuth (deg)
- 6
0
+ 6
24
12
0
B
H028
25
12.5
0
C
H026
47
23.5
0
D
CH017
29
14.5
0
E
CH006
38
19
0

Figure 3

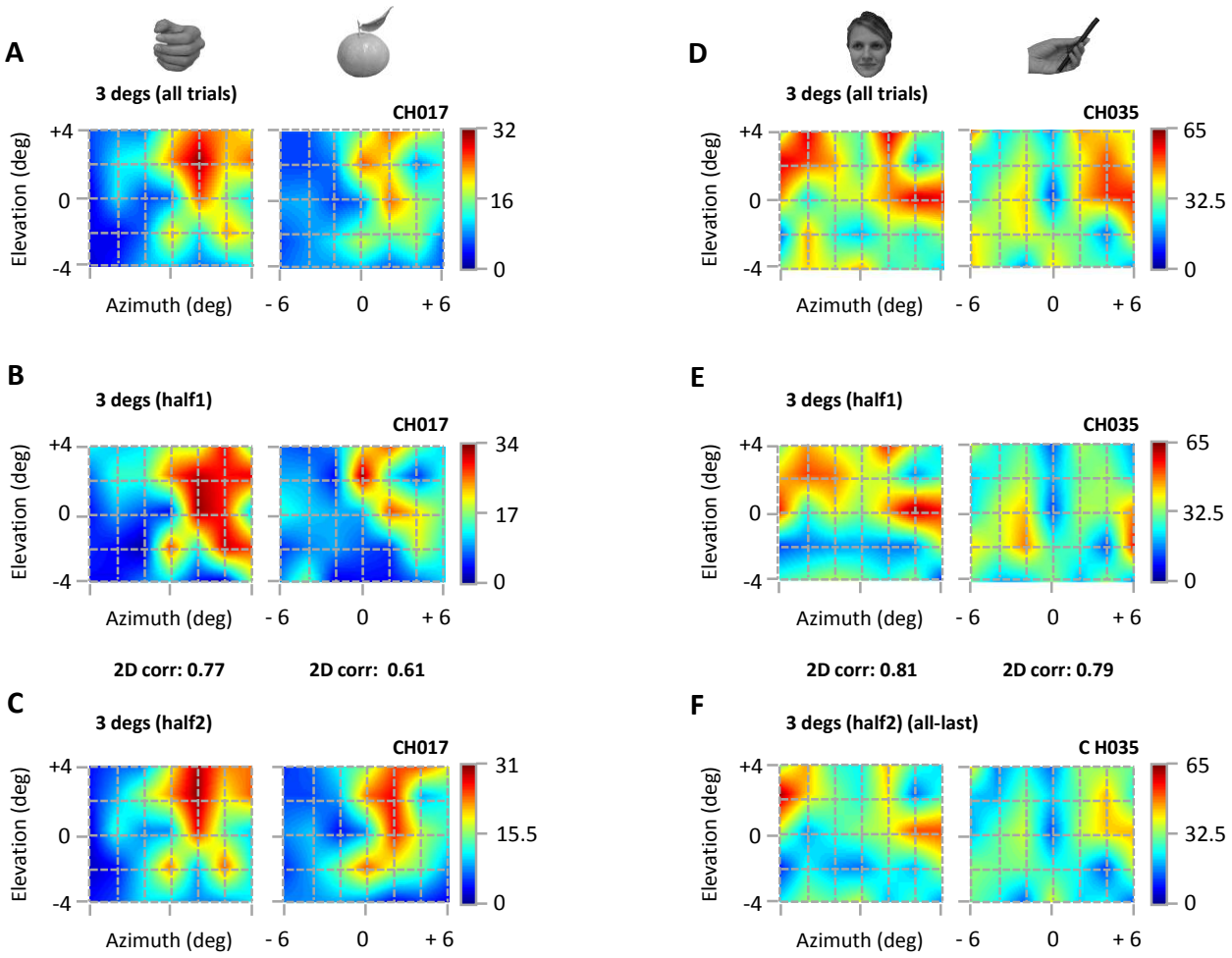
A
3 degs (all trials)
CH017
Elevation (deg)
+4
0
-4
Azimuth (deg)
- 6
0
+ 6
32
16
0
B
3 degs (half1)
CH017
34
17
0
2D corr: 0.77
C
3 degs (half2)
CH017
31
15.5
0
D
3 degs (all trials)
CH035
65
32.5
0
E
3 degs (half1)
CH035
65
32.5
0
2D corr: 0.81
2D corr: 0.79
F
3 degs (half2) (all-last)
C H035
65
32.5
0

Figure 4

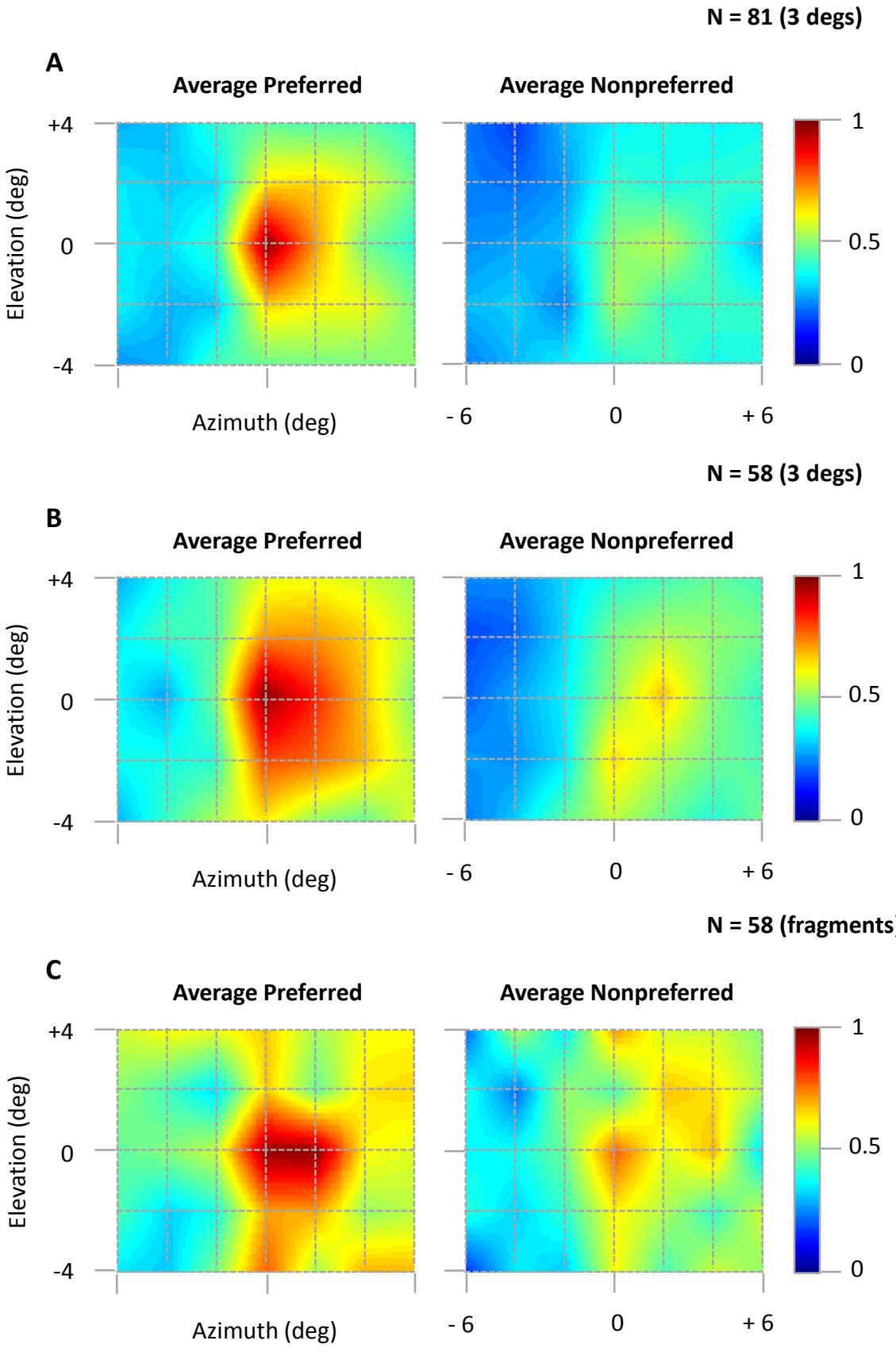
N = 81 (3 degs)
A
Average Preferred
Average Nonpreferred
+4
0
-4
Elevation (deg)
Azimuth (deg)
- 6
0
+ 6
1
0.5
0
N = 58 (3 degs)
B
Average Preferred
Average Nonpreferred
+4
0
-4
Elevation (deg)
Azimuth (deg)
- 6
0
+ 6
1
0.5
0
N = 58 (fragments)
C
Average Preferred
Average Nonpreferred
+4
0
-4
Elevation (deg)
Azimuth (deg)
- 6
0
+ 6
1
0.5
0

Figure 5

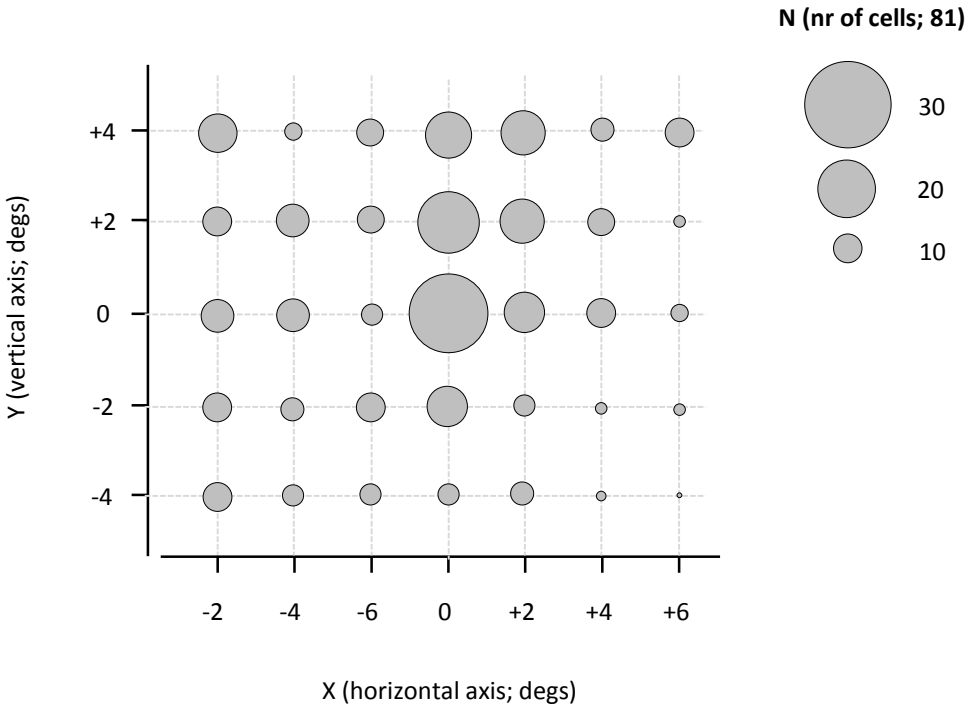
N (nr of cells; 81)
30
20
10
+4
+2
0
-2
-4
Y (vertical axis; degs)
-2
-4
-6
0
+2
+4
+6
X (horizontal axis; degs)

Figure 6

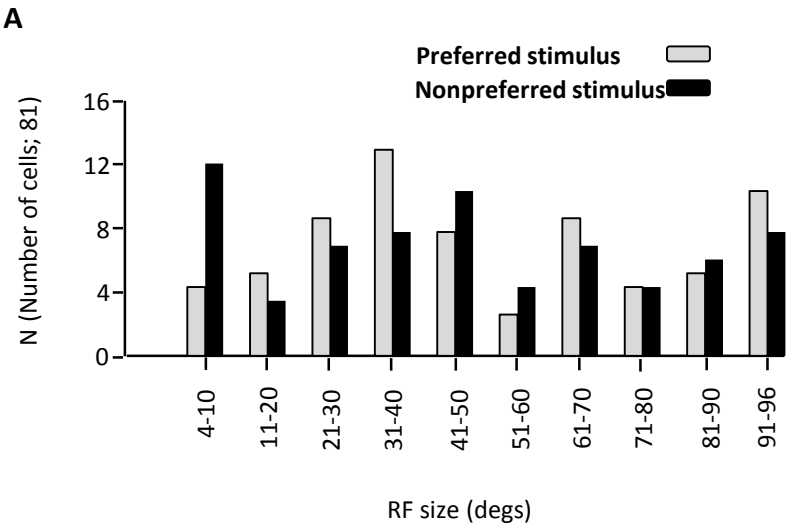
A
Preferred stimulus
Nonpreferred stimulus
N (Number of cells; 81)
16
12
8
4
0
4-10
11-20
21-30
31-40
41-50
51-60
61-70
71-80
81-90
91-96
RF size (degs)

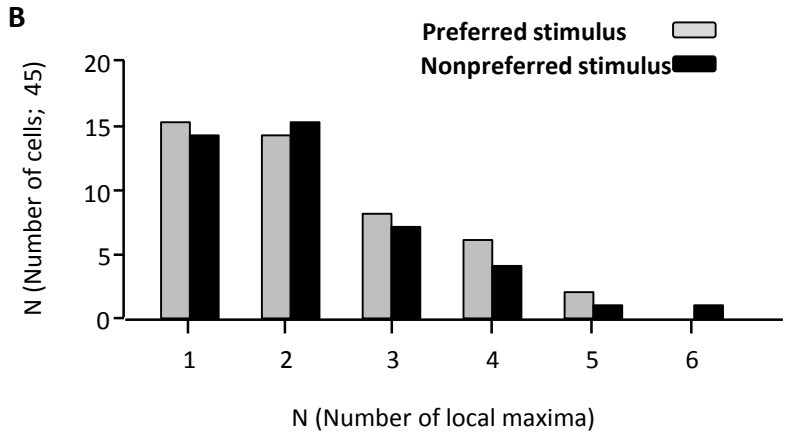
B
Preferred stimulus
Nonpreferred stimulus
N (Number of cells; 45)
20
15
10
5
0
1
2
3
4
5
6
N (Number of local maxima)

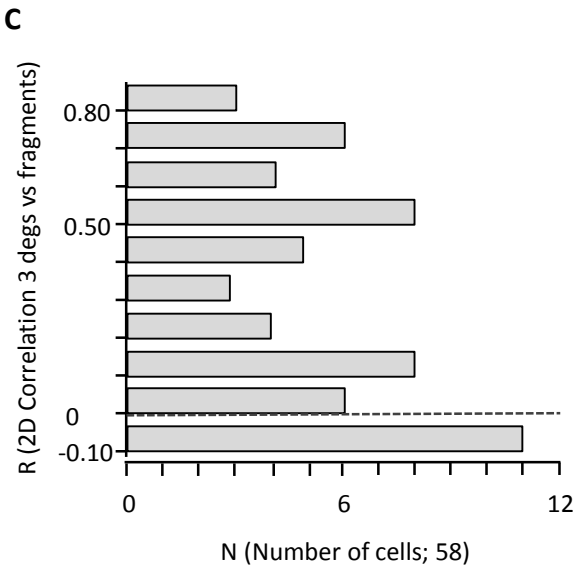
C
R (2D Correlation 3 degs vs fragments)
0.80
0.50
0
-0.10
0
6
12
N (Number of cells; 58)

Figure 7

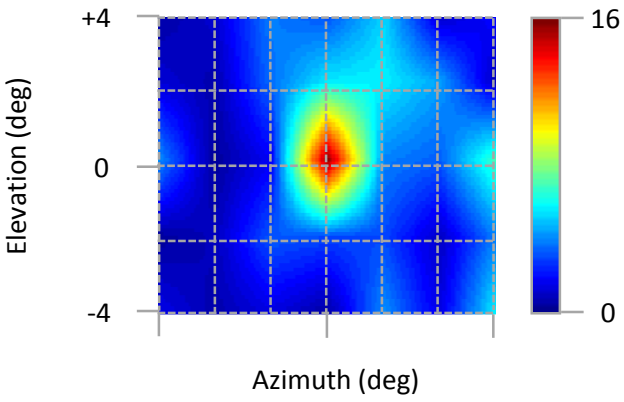

Figure 8

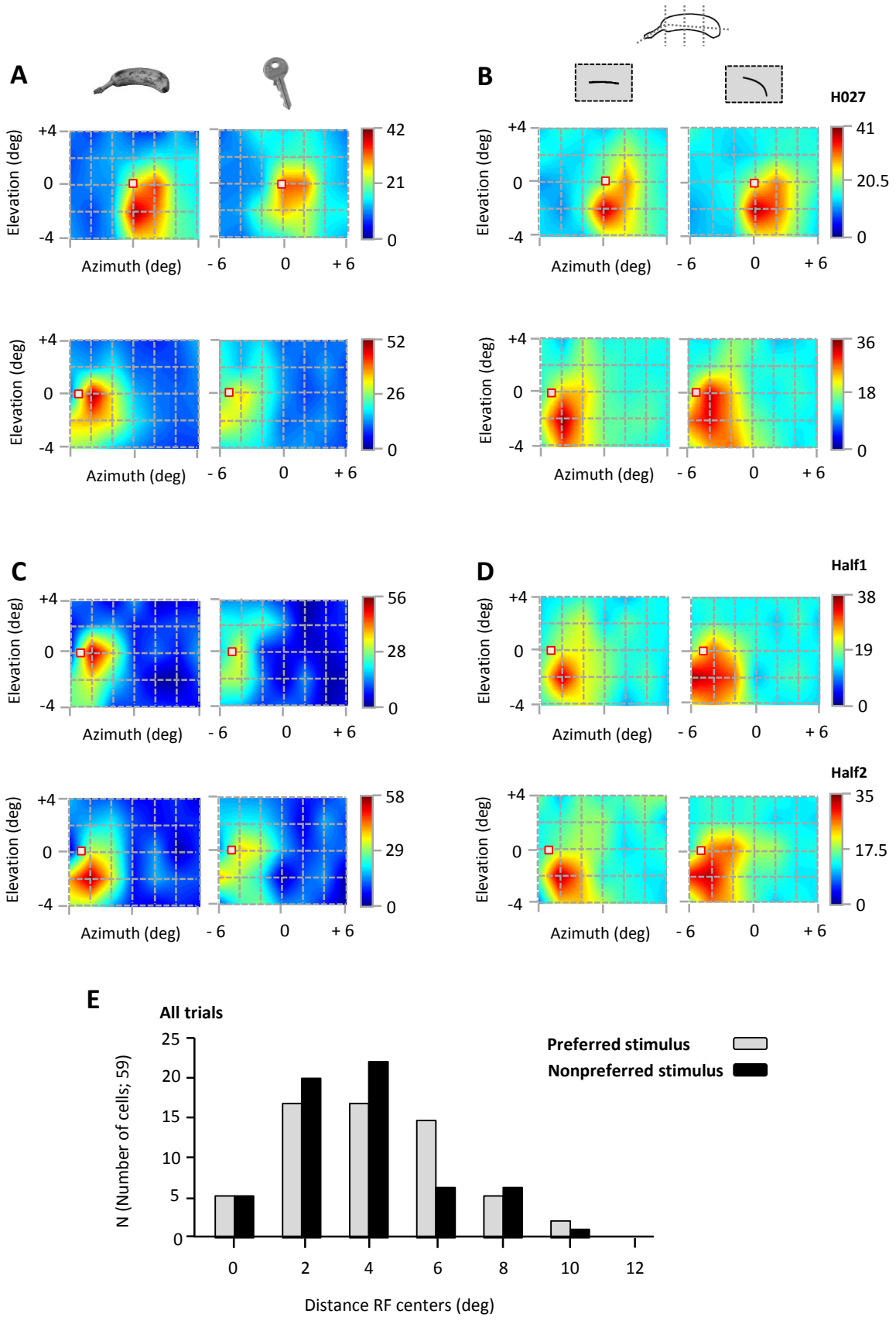
A
B
H027
C
D
Half1
Half2
Elevation (deg)
Azimuth (deg)
+4
0
-4
- 6
+ 6
42
21
41
20.5
52
26
36
18
56
28
38
19
58
29
35
17.5
E
All trials
Preferred stimulus
Nonpreferred stimulus
N (Number of cells; 59)
Distance RF centers (deg)
25
20
15
10
5
0
2
4
6
8
10
12

Figure 9

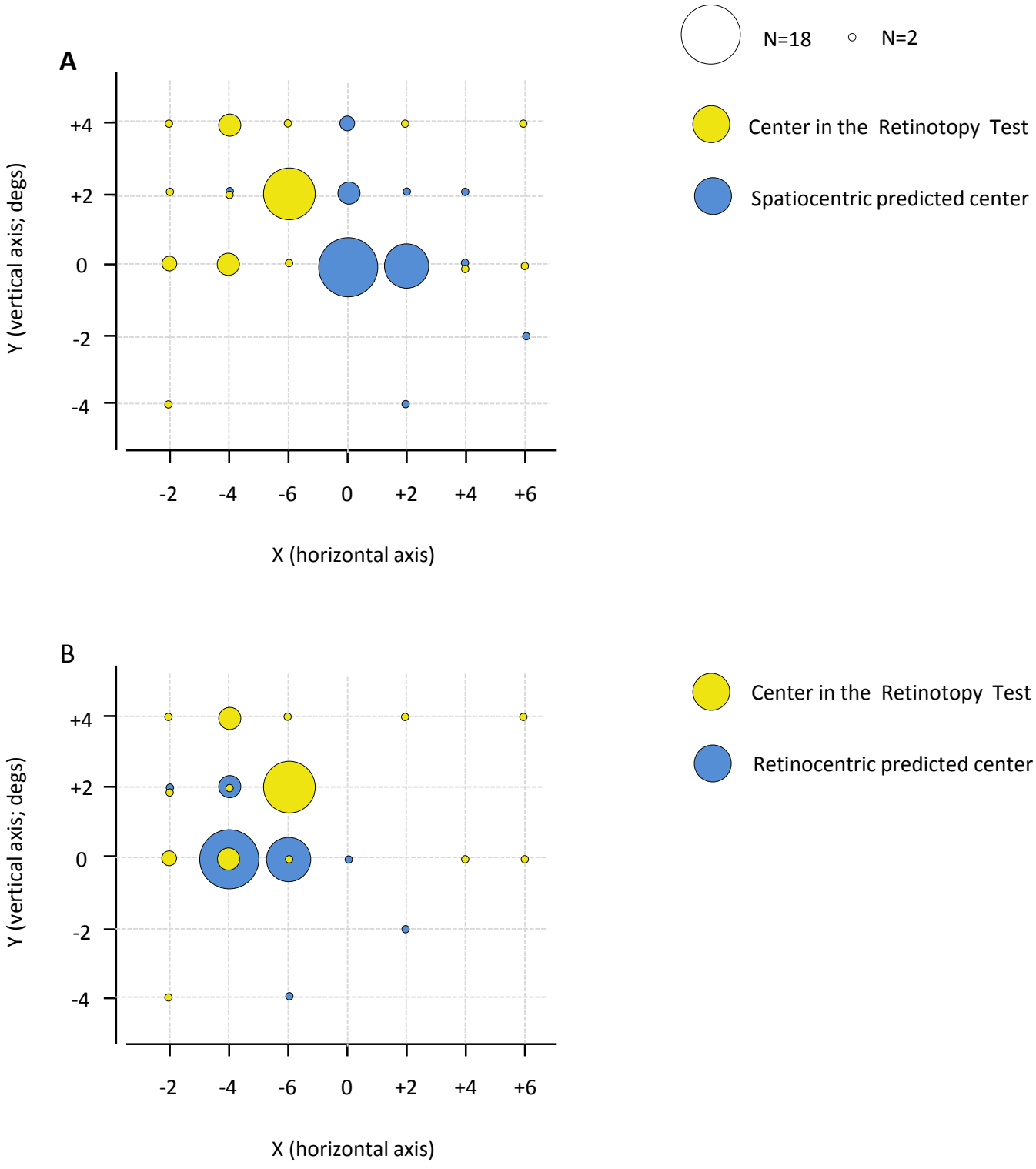
A
N=18
N=2
Center in the Retinotopy Test
Spatiocentric predicted center
+4
+2
0
-2
-4
Y (vertical axis; degs)
-2
-4
-6
0
+2
+4
+6
X (horizontal axis)
B
Center in the Retinotopy Test
Retinocentric predicted center
+4
+2
0
-2
-4
Y (vertical axis; degs)
-2
-4
-6
0
+2
+4
+6
X (horizontal axis)

Figure 10